SAFE NATURAL FAR RENDEZVOUS APPROACHES FOR CISLUNAR NEAR RECTILINEAR HALO ORBITS IN THE EPHEMERIS MODEL

Emmanuel Blazquez, Laurent Beauregard, Stéphanie Lizy-Destrez

Institut Supérieur de l'Aéronautique et de l'Espace (ISAE-SUPAERO)
Department of Aerospace Vehicles Design and Control
10 avenue Edouard Belin 31400 Toulouse, France

ABSTRACT

In the context of future Human Spaceflight exploration missions, Rendezvous and Docking (RVD) operational activities are mandatory and critical for the assembly and maintenance of cislunar structures. The scope of this research is to investigate the specifics of orbits of interest for RVD in the cislunar realm and to propose innovative strategies and trajectory designs to safely perform far rendezvous operations. With a focus on Near Rectilinear Halo Orbits (NRHO), this work investigates passively safe drift trajectories in the Ephemeris model in order to exhibit phasing orbit requirements to ensure safe far approach while admitting low-cost transfer capabilities.

Index Terms— Rendezvous, EML2, Near Rectilinear Halo Orbits, Trajectory design, Safety

1. INTRODUCTION

Rendezvous and Docking (RVD) operational activties are mandatory and critical for cargo delivery and crew echange missions targeting a cislunar infrastructure, such as the future Lunar Orbital Platform-Gateway (LOP-G) [1, 2]. There is extensive experience with RVD in the two-body problem in Low Earth and Lunar Orbits and to various space stations, based on the Apollo missions or the ATV deliveries to the ISS. Despite that, the problem of RVD in non Keplerian dynamics is a quite recent topic and no operational rendezvous has yet been performed in the vicinity of the Lagrangian points.

In recent years, an emergence of publications on the subject of RVD in the cislunar realm has been observed, often related to studies focusing on the LOP-G and Orion missions. [3, 4] Near Rectilinear Halo Orbits (NRHOs) have been identified as suitable locations for placing large cislunar infrastructures and for multi-mission staging, due to their attractive eclipse avoidance properties and relative easy access and departure [5].

The scope of this paper is to investigate the specifics of orbits of interest for RVD in the cislunar realm and to propose innovative strategies and trajectory designs to safely perform far rendezvous approaches in such a complex environment. With a focus on NRHOs about the L2 Earth-Moon Lagrangian point (EML2), previous work has investigated close rendezvous relative dynamics using linear and non-linear targeting algorithms [6]. This work focuses on natural far approach and the investigation of passively safe drift trajectories in the Ephemeris model. The goal is to exhibit phasing orbit requirements, given a prescribed target orbit, that ensure safe free motion and natural approach of a spacecraft near the target.

First, the formulation of the equations of motion in both the CR3BP and the full Ephemeris model is analyzed. These results are then used to construct long term pseudo-stable orbits by means of multiple shooting differential correction and adaptive long-horizon targeting algorithms. The non-linearity of the Ephemeris model leads to quasi-periodic NRHO-like trajectories naturally drifting with respect to their CR3BP counterparts. This natural drift is then exploited to achieve natural approach of the chaser to the target. Different phasing orbits are compared depending on the radius of their perilune, and classified according to their natural approach capabilities. Finally, safety issues are adressed using impact prediction strategies derived from debris avoidance analysis. A general methodology to design safe free drift approach for RVD in the ephemeris model is thus presented.

2. DYNAMICAL MODELS

2.1. The Circular Restricted Three-body Problem (CR3BP)

The CR3BP describes the motion of a massless particle P under the gravity field created by two massive primary bodies, P_1 and P_2, assumed to be punctual and with masses m_1 and m_2 respectively. Both P_1 and P_2 are in a circular motion around their center of mass. By convention, $m_1 > m_2$ and the mass parameter $\mu = \dfrac{m_2}{m_1 + m_2}$ is introduced. A synodical, barycentric rotating reference frame $\mathcal{R}(O, xyz)$, with its origin at the center of mass of the system, is adopted. The system is also made nondimensional using appropriate normalizing length and time. One can refer to [7] for a detailed

description of the problem.

The second-order equations of motion of P in the synodic frame are:

$$\begin{cases} \ddot{x} - 2\dot{y} = U_x \\ \ddot{y} + 2\dot{x} = U_y \\ \ddot{z} = U_z \end{cases} \quad (1)$$

where $U(x,y,z) = \frac{x^2+y^2}{2} + \frac{1-\mu}{r_1} + \frac{\mu}{r_2} + \frac{\mu(1-\mu)}{2}$, U_x, U_y and U_z are the partial derivatives of U with respect to x, y and z, and $r_1 = \sqrt{(x+\mu)^2+y^2+z^2}$, $r_2 = \sqrt{(x-1+\mu)^2+y^2+z^2}$.

2.2. The Ephemeris Model

The Ephemeris model is commonly referred to as the *Solar System N-Body Problem*. The orbits of the primaries are no longer planar nor periodic, but are given by ephemeris of the precise positions and velocities of the bodies over time.

The motion of a massless point P under the influence of $N-1$ massive primaries, of masses m_1,m_2,...,m_{N-1} respectively, is given by the second order differential equation:

$$\ddot{\mathbf{X}} = -\mu_1 \frac{\mathbf{X}}{||\mathbf{X}||^3} - \sum_{i=2}^{N-1} \mu_i \left(\frac{\mathbf{X}-\mathbf{X}_i}{||\mathbf{X}-\mathbf{X}_i||^3} + \frac{\mathbf{X}_i}{||\mathbf{X}_i||^3} \right) \quad (2)$$

where μ_i is the standard gravitational parameter of the i-th primary, defined as $\mu_i = G \cdot m_i$, G is the gravitational constant and $\mathbf{X}_i$ is the position vector of the i-th primary. The force model is purely newtonian. The equations of motion are formulated in an inertial frame and describe the state of the spacecraft $\mathbf{X}(t)$ relative to the position of a primary (by convention, the first primary of the N-body system is chosen). This formulation can be modified to take into account additional perturbations, such as the solar radiation pressure or non-uniformities in gravity fields of the primaries.

This study includes the influence of the Moon, Earth and Sun modeled as point masses using the gravitational parameters shown in Table 1. The motion of the primaries are extracted from the DE421 Ephemeris of the *Jet Propulsion Laboratory* (JPL), embedded in the SPICE Toolkit [8].

Table 1. Gravitational parameters (from DE421 [8])

Primary	μ (km^3/s^2)
Earth	3.9860043623×10^5
Moon	4.902800076×10^3
Sun	$1.32712440040944 \times 10^{11}$

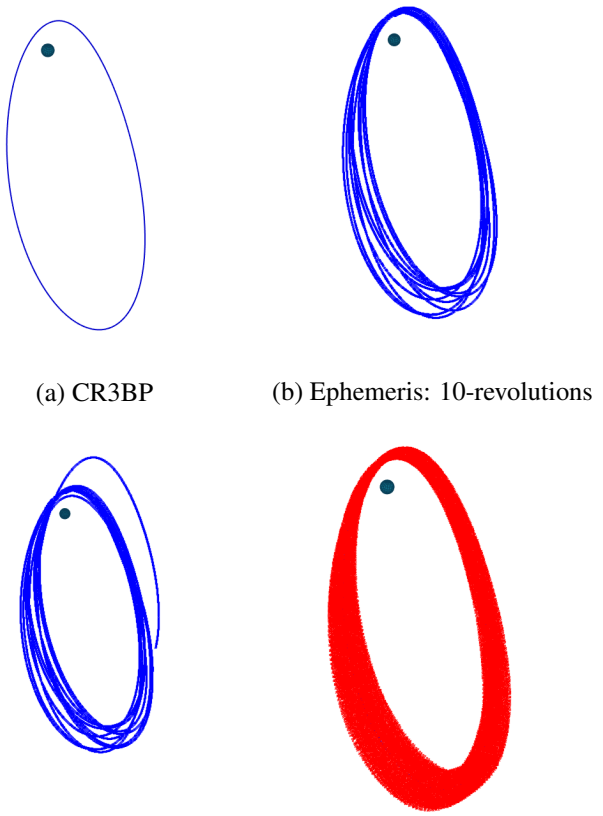

(a) CR3BP (b) Ephemeris: 10-revolutions

(c) 100 days no correction (d) Ephemeris: 500-revolutions

Fig. 1. Southern EML2 NRHO with $r_p = 5930\ km$ in different dynamical models, represented in the synodic frame (CR3BP) or pseudo pulsating frame (Ephemeris)

3. GENERATING NRHOS IN THE EPHEMERIS

This section describes the methodology applied to obtain orbits with NRHO-like motion in the Ephemeris model described in section 2.2. The methodology consists in starting from an NRHO solution of the CR3BP and differentially correcting it in the Ephemeris model. The process will be briefly described here, one can refer to [9, 10] to learn more about the generation of CR3BP orbits and their transition to the Ephemeris model.

3.1. NRHOs in the CR3BP

NRHOs are a subset of Halo orbits, named after their elongated shape and quasi-perpendicular orientation with respect to the plane of motion [11]. This work focuses on Southern EML2 NRHOS, characterized by by an apolune passing over the lunar south pole and a low perilune radius. In the CR3BP, NRHOs are periodic orbits.

The usual methodology to obtain such orbits is to use an appropriate first guess of a periodic solution in the linearized

CR3BP [12] and apply diferential correction to the initial state of the orbit to enforce periodicity [13]. Figure 1.a shows an example of a Southern EML2 NRHO in the synodic frame.

Typically Halo orbits are constructed and classified according to their out-of-plane amplitude A_z. However, since EML2 NRHOs are characterized by their close approach to the Moon at the perilune, it is more convenient to classify them by perilune radius r_p.

3.2. Transition to the Ephemeris

In the Ephemeris model, NRHOs are no longer periodic but quasi-periodic, due to the highly non-linear dynamics involved. In order to preserve the stability and coverage properties of such orbits, it is paramount to ensure a soft transition to the Ephemeris model. In addition, the close approach to the Moon leads to very fast dynamics near the perilune with great dispersion of velocity increments. This translates into difficulties to converge for numerical solvers such as classical differential correctors.

NRHOs computed in the CR3BP provide an accurate initial guess for transition to the Ephemeris model. In order to perform the correction, an epoch-varying multiple shooting differential corrector is employed, with additional constraints added to ensure epoch continuity [9]. The solution obtained is indeed ballistic and quasi-periodic (Figure1.b) but diverges after roughly 90 to 100 days (Figure1.c): preserving NRHO-like motion requires additional stationkeeping.

In order to generate long-term stable orbits, another correction process must be added to the procedure. For this work, an adaptive Long-Horizon (or Receding-Horizon) correction scheme was applied [14, 5]. The ballistic trajectory obtained with the multiple-shooting correction is used to initalize the long-horizon procedure. In the CR3BP, Halo orbits are characterized by a velocity $v_x = 0$ at the $y = 0$ plane crossing. The long-horizon correction algorithm starts from the perilune of the orbit and propagates for a number N_{LH} of revolutions downstream until the $y = 0$ plane crossing is reached. It then performs differential correction on the velocity component of the state vector at the perilune to enforce $v_x = 0$ at the end of the propagated state. The new obtained orbit is guaranteed to be stable for at least N_{LH} revolutions. The new initial state is propagated till the next perilune, and the process is repeated until a satisfying number of stable revolutions are achieved.

The choice of the N_{LH} parameter is paramount: in order to reduce the ΔV cost for stationkeeping, velocity increments at the perilune must be lowered as much as possible. Higher values of N_{LH} lead to lower correction velocities (shown in Table 2), but in return result in higher computational strain. This works proposes the use of an adaptive long-horizon approach, with N_{LH} varying depending on the orbit propagated. The user specifies a maximum ΔV_{max} amplitude of maneuver for each single event at the periapsis, and the algorithm selects the best long horizon parameter based on a series of 10 revolution simulations. Starting from $N_{LH} = 5$, maneuvers are computed. If at some point during the test propagation a maneuver exceeds ΔV_{max}, the process is interrupted and re-initiated with $N_{LH} = N_{LH} + 1$, until the maximum maneuver amplitude condition is verified. For this work, $\Delta V_{max} = 1\ mm \cdot s^{-1}$. This protocol is especially advantageous when trying to propagate orbits for large time scales (>1 year), and typically for $2000\ km < r_p < 6500\ km$ come parameters in the $5 < N_{LH} < 11$ range. Using this methodology the orbit maintenance budget for a 500-revolution NRHO-like motion with $r_p = 5930\ km$ ($\simeq$ 10 years) is equal to 61.729 mm/s, with a maximum maneuver amplitude of 0.518 mm/s. These values are consistent with the ones found in the literature [5].

Table 2. Variation of stationkeeping ΔV depending on N_{LH}, for $r_p = 5930\ km$ and 10 revolutions

N_{LH}	ΔV_{max} (mm/s)	ΔV_{total} (mm/s)
8	4.15	6.00
9	0.77	1.62
10	0.36	0.64

4. NATURAL DRIFT AND FAR RENDEZVOUS

As an extension of successful rendezvous operations performed in Low Earth Orbit, it is possible to identify three successive phases in rendezvous operations: the transfer phase, the far rendezvous and the close rendezvous. This work focuses on the far rendezvous operations: taking place after the spacecraft has been injected into a proper phasing orbit. This section details how to use the natural drift of Ephemeris NRHOs with respect to their reference in the CR3BP to achieve natural far RVD.

4.1. Study case

In the following analysis, the term "chaser" refers to the spacecraft performing the maneuvers to reach the "target" orbiting infrastructure, placed on a Southern NRHO about EML2. For this study, a perilune radius $r_{p,target} = 5930\ km$ was chosen for the target orbit. This choice is driven by accessibility constraints from both LLOs and LEOs, low unstability properties and a 4:1 resonance with the lunar synodic cycle. Such an orbit could indeed, with proper phasing and orientation, ensure eclipse avoidance for extended periods of time [4, 5]. However, the methodology presented in this paper is applicable to target NRHOs of different perilune radii without exception. The chaser is placed on a Southern EML2 NRHO with varying perilune parameter $r_{p,chaser}$. The reference epoch orbit generation is set to *2025 NOV 8 23:22:07*. Far rendezvous occurs before close proximity operations begin (final approach, docking/berthing, etc.) and given the

distance between chaser and target relies on absolute navigation for the most part (above 75-100 km).

As shown in Figure 1.b NRHOs are no longer periodic in the Ephemeris and tend to hover around their reference CR3BP counterpart in a pseudo-pulsating frame, N-body equivalent of the synodic frame [15]. Starting from an $r_p = 5930\ km$ target orbit, the idea is to see how the drifts of both the target and nearby candidate phasing orbits overlap, and exploit these properties to achieve safe natural approach as shown in Figure 2.a.

Two different regions shall be investigated. The *approach region* corresponds to candidates within a distance $75\ km < d < 100\ km$ of the target orbit. Such boundaries are chosen because they typically correspond to the range at which RF ranging can be intiated [16]. The *safety region* is defined within a radius of $50\ km$ around the target orbit. This region identifies potentially dangerous candidates (collision threats) that should be treated separately and will be discussed in Section 5.

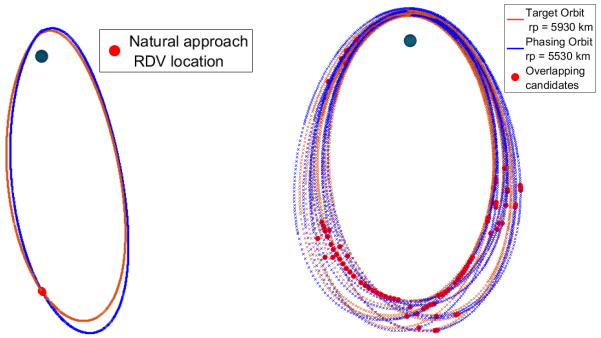

(a) Natural far rendezvous (b) Local plane search

Fig. 2. Natural far rendezvous locations

4.2. Natural drift approach: candidate search

Not all locations in an NRHO are suited to start close-proximity maneuvers. Close passage to the Moon at the perilune comes with very fast dynamics. This is problematic for three main reasons. The first is the duration of the rendezvous operations that is not negligible with respect to the amount of time spent near the perilune. Another reason prescribing rendezvous at the perilune is the large dispersion maneuver that can result from maneuver failures or inappropriate state estimation in the area. Finally, in case of an important failure involving large drifts of the spacecraft, the chaser would then be hovering in an uncertain manner near the Moon with therefore higher probability of entering trajectories quickly impacting with the Moon surface or other infrastructures placed on Low Lunar Orbits. For all these reasons RVD operations should take place as close as possible from the apolune of the NRHOs.

When looking at the drifting trajectories and possible close encounter candidates resulting from this free motion, it is thus useful to classify them depending on their angular location. Let us call $\theta \in [0; 2\pi]$ the angular parameter giving the location of a spacecraft on its corresponding NRHO, defined with respect to the appropriate pseudo center so that $\theta = 0$ at the perilune and $\theta = \pi$ at the apolune, and with respect to the z axis of the Earth-Moon pseudo-pulsating frame.

- Locations with $\theta < \pi/2$ and $\theta > 3\pi/2$ are considered near-perilunar and therefore discarded for RVD activities
- Locations with $\pi/2 < \theta < 3\pi/2$ should be considered as potential candidates for RVD operations. Specifically cases with $3\pi/4 < \theta < 5\pi/4$, defining near-apolunar regions, are of special interest.

A first way to find potential overlapping drift candidates with very little computational effort is to apply a local-plane crossing search procedure. For each point of the propagated target orbit, a local plane is defined using its two nearest neighbors. If $\mathbf{x}_{t,k}$ is the position vector corresponding to the k-th point of the target orbit, the local plane is defined on point $\mathbf{x}_{t,k}$ using the vectors $(\mathbf{x}_{t,k+1} - \mathbf{x}_{t,k}, \mathbf{x}_{t,k} - \mathbf{x}_{t,k-1})$. If at some point in the chaser orbit two consecutive states $\mathbf{x}_{c,i+1}$ and $\mathbf{x}_{c,i+1}$ are found on different sides of the nearest local plane of the target orbit, then a single distance check gives information on the dangerosity or interest of the location. Figure 2.b gives an example of such a search performed with a chaser orbit with $r_p = 5530\ km$ and neighbors nearest than 50 km.

The local plane search method, however, can only give a rough estimation of potential candidates and should only serve to quickly find an order of magnitude for the number of potential points of interest or dangerosity for natural RVD.

Two other alternatives exist. The first is a simple nearest neighbor search performed over all the propagated points of the orbits. The other, more computationally demanding, requires to first define a cylinder around the target orbit. The radius of the cylinder corresponds to the radius of search for overlapping candidates. The surface obtained is then triangulated using Delaunay triangulation [17] and points in the chaser orbits are then investigated to see if they belong inside the newly defined volume. Alternatively, such a cylinder can also be constructed for the chaser orbit and the candidates found looking at the intersection of two Delauney surfaces. The use of such tubes is only really recommended when the resolution of the orbit is not high enough and interpolation is required. Even though the process of accessing Delaunay triangulations of both chaser and target tubes can be computationally demanding, for long-duration orbits it can be faster than refining the Ephemeris orbit to add more query points.

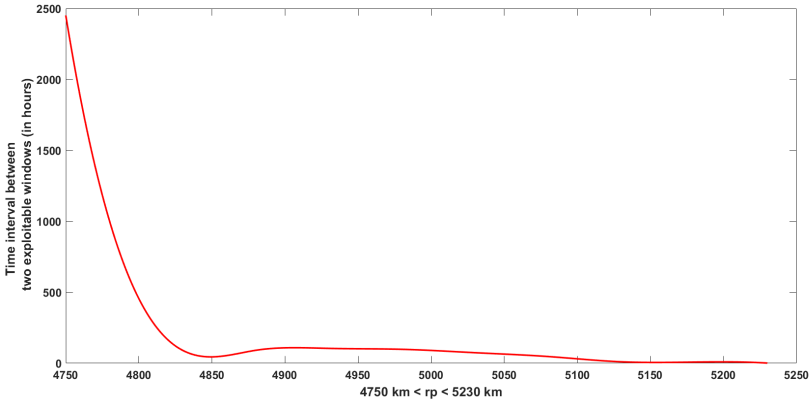

(a) Full distribution

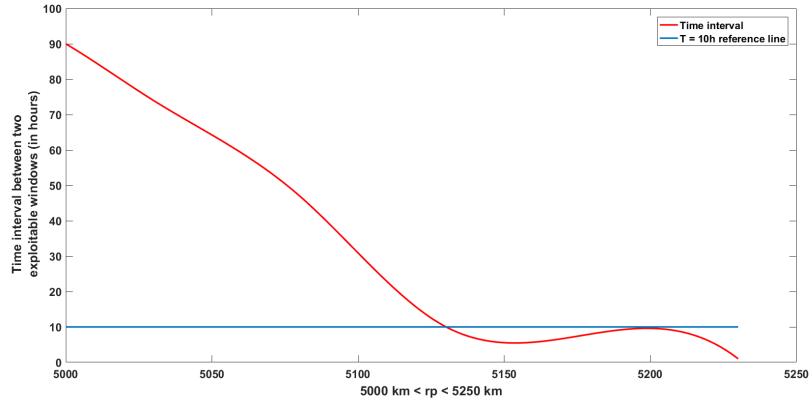

(b) Zoom at $5000\ km \leq r_p \leq 5230\ km$

Fig. 3. Minimum time between two natural RVD windows

4.3. Natural drift approach: analysis

Figure 4 shows the number of potential RVD candidates and perilune encounters depending on the perilune radius of the phasing NRHO, after 10 revolutions of the target orbit. For orbits with $r_p < 4330\ km$, no candidates are within the approach region defined in Section 4.1. Obviously, as $r_{p,chaser}$ grows and tends towards $r_{p,target}$, the number of encounters exponentially grows. The objective here is twofold: ensure the phasing orbit offers enough encounter possibilities within the approach tube and avoid as much as possible periapsis encounter candidates which represent possible hazardous situations at the perilune where maneuvers should be avoided as much as possible. For this study's target orbit, the exponential growth for periapsis encounters starts skyrocketing at $r_p \simeq 5300\ km$. This perilune value should therefore be considered an upper boundary for the chaser orbit perilune if one wants to take advantage of the natural approach. For chaser orbits with $r_p \leq 4550\ km$ no overlapping of the chaser NRHO with the target orbit occurs within the approach region. Such orbits offer no natural far rendezvous opportunities and can therefore be discarded for the present study. The domain under consideration for the chaser orbit is therefore $4550\ km \leq r_p \leq 5300\ km$.

A trade-off becomes apparent here: the more the chaser orbit will tend towards the upper bound, the more rendezvous opprtunities there will be, but the more hazardous cases will need to be investigated near the perilune. It is important to note that, if the far rendezvous succeeds, these encounters are a non-issue because they happen after the first revolution of the chaser has taken place. But in case of a no-go or if the RVD is postoponed, they become possibly hazarduous situations that need to be taken into account. Three criteria should drive decision-making at this point: safety considerations (discussed in Section 5), budget for transition to proximity operations (Section 4.4) and finally opportunity window recurrence.

Opportunity window recurrence refers to both the delay necessary to reach another rendezvous opportunity in case of a no-go, and the duration of the opportunity window. Fig-

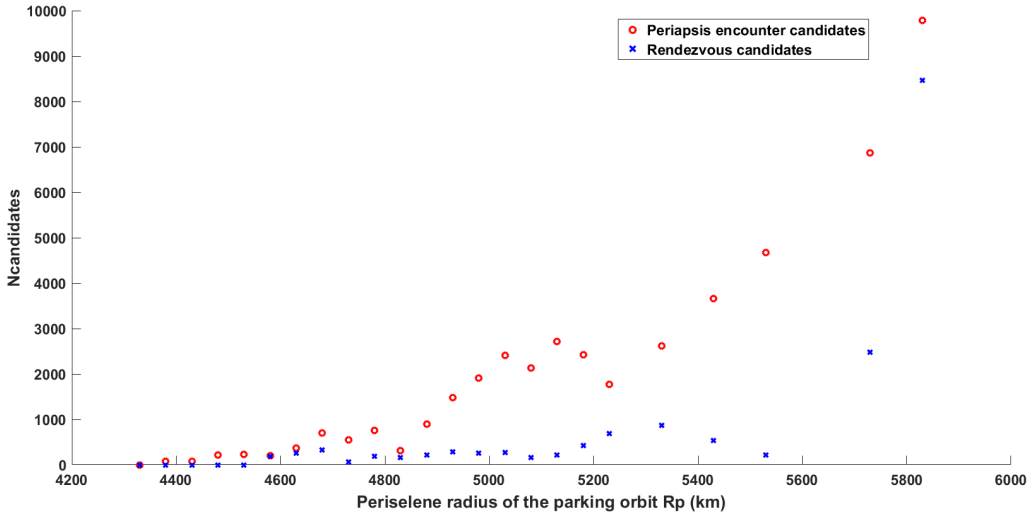

Fig. 4. Distribution of natural far RVD candidates with respect to perilune radius of the chaser orbit, after 10 revolutions of the target orbit

ure 3 represents the minimum time between two exploitable windows as a function of the perilune radius of he chaser orbit. For the studied target orbit and within the $4550\ km \leq r_p \leq 5300\ km$ range defined for the chaser orbit, four different cases are observed:

- $r_p \leq 4750\ km$: No interesting windows: short durations (maximum of 30 minutes) and very long wait in between two windows.
- $4750\ km \leq r_p \leq 5000\ km$: Opportunity windows last in average 1 hour, but because the wait time between windows is quite high (100 hours average) only one opportunity can be reasonably exploited.
- $5000\ km \leq r_p \leq 5100\ km$: Most suited range for cargo/uninhabited missions with weak time-of-flight constraints. Windows last between 1 and 2 hours with typical times in betwen windows of 23 to 72 hours. For instance $r_p \simeq 5080\ km$ provides 2 opportunity windows of durations 1.08 h and 3.45 h respectively, with a wait time of 48h.
- $5100\ km \leq r_p \leq 5300\ km$: Range suitable for for both cargo and possibly manned flights. Opportunities tend to last between 1 and 6 hours with relatively short wait times. A good example is provided by the $r_p \simeq 5230\ km$ chaser orbit. Two windows of 1.03 h and 2.13 h respectively are separated by a wait time of ~ 1 h. In case of two consecutive no-gos at those windows, a re-phasing maneuver performed a the periapsis will provide access to two other opprtunities, of 1.11 and 0.21 h respectively, separated by a duration of 0.14 h.

4.4. Transition to close proximity operations, low-transfer capabilities

Once the chaser has entered the approach zone and is therefore in proximity of the target, different scenarios can be considered. The tradeoff between the different options available is beyond the scope of this work and will be part of future publications. One option is to consider ending the far-rendezvous and initiating proximity and close operations protocols. This is of course subject to the validty of relative models and relative navigation measurements within the approach sphere domain. The other option is to engage a transition between far and close rendezvous by adding two maneuvers. The transfer can be computed using Lambert arcs in the Ephemeris, similarly to the computation of a trajectory correction maneuver. One could also revert to the three body representations of target and chaser orbit in the approach zone and exploit the invariant manifolds of the orbits to find low-energy transfers within this domain.

5. SAFETY ANALYSIS AND PHASING ORBIT SELECTION

The orbits described and selected in Section 4 must also be analyzed from a safety point of view. Section 4.2 established that natural approach trajectories have the chaser spacecraft enter the so-defined safety region of the target. One must ensure that such events do not present any major risk of encounter between the two objects, in order to reduce the occurence of collision avoidance maneuvers in case of a no-go. This section details the safety analysis of such possible encounters, that happen when the chaser enters a tube

of radius $r = 50\ km$ around the target, following its trajectory. This safety analysis will focus on chaser orbits in the $4750\ km \leq r_p \leq 5300\ km$ range, as they were shown to be the most interesting locations for natural far rendezvous approach (Section 4.3).

5.1. Covariance ellipses, probability of collision

This work makes use of estimation techniques for conjunction threats commonly used for debris-avoidance analysis. It is based on the works of Alfano, Oltrogge, Chan and al. [18, 19, 20] A brief summary of the concepts used in this work will be presented for completion's sake.

Probability of collision P_c is a useful and popular tool to assess conjunction threats. Relying on proabbilistic theory, it makes use of concepts such as miss distance and covariance noise to establish the probability of two objects encountering, each following its own independent trajectory.

The following simplifying assumptions are made:

- Chaser and target are modelled as two spherical objects (of respective radii R_c and R_t), and the relative motion of the target with respect to the chaser is observed: the chaser is fixed in this new local reference frame.
- Relative motion of chaser and target is fast enough within the encounter time to be considered linear.
- Positional noises are zero-mean, Gaussian and uncorrelated.
- The covariance matrix is considered constant during the encounter.

In such a model, the uncertainty in chaser and target position is modelled by two covariance ellipsoids centered on their respective bodies. Given a covariance matrix Σ, and a body position vector $\boldsymbol{\mu}$, the covariance ellipsoid can be defined as the set:

$$\epsilon = \{\mathbf{x} : (\mathbf{x} - \boldsymbol{\mu})^T \Sigma^{-1} (\mathbf{x} - \boldsymbol{\mu}) \leq \chi\} \tag{3}$$

where χ is the value of a chi-square distribution with three degrees of freedom, and defines the percentage of the probability distribution contained within the ellipsoid.

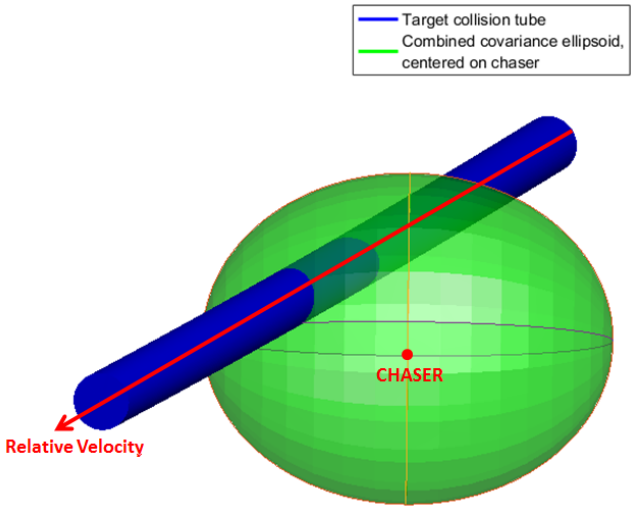

Fig. 5. Modeling of an encounter in the approach region

In the chaser-local reference frame, the target's linearized motion is represented as a tube. Collision occurs if the difference in position between chaser and target is less than the sum $R_c + R_t$. The probability of collision is computed as the integral of the three-dimensional probability density function over the target tube. From the two covariance ellipsoids attributed to each object, and because noises are uncorrelated, one can build a combined covariance ellipsoid centered on the chaser. The modeled encounter in the approach region is shown in Figure 5.

Numerical methods to evaluate the probability integral exist, however it is possible to obtain quite easily an upper boundary for P_c. For a given aspect ratio $AR \geq 1$ of the combined ellipsoid projected in the encounter plane, the maximum probability of collision is given by:

$$P_{c,max} = \left(\frac{\alpha}{1+\alpha}\right)\left(\frac{1}{1+\alpha}\right)^{\frac{1}{\alpha}} \tag{4}$$

where $\alpha = \dfrac{(r_c + r_t)^2 AR}{d^2_{target-chaser}}$

5.2. Safety results

The maximum probability of collision is computed for each set of encounter candidates and for two different types of error in position determination: one with $3\sigma = 1\ km$ (small error) and one with $3\sigma = 10\ km$ (medium error). In equation 3, the value of χ is set to 7.815 to account for 95% of the probability distribution. The target is asummed to be a space station with dimensions comparable to the ISS, modeled as a sphere of radius $110\ m$. The chaser is modeled as $10\ m$ radius sphere (dimensions comparable to the length of ESA's Automated transport Vehicle).

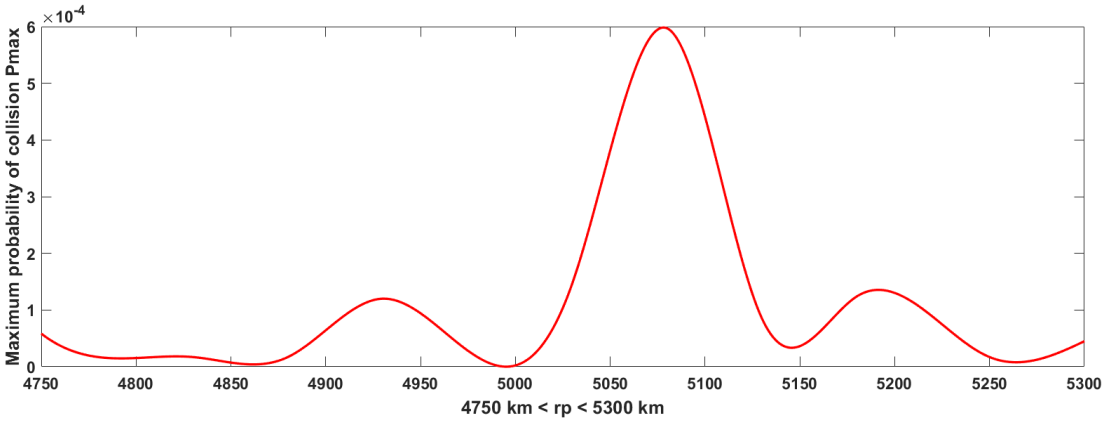

Fig. 6. Maximum probability of collision in the safety region for different perilune radii of the chaser orbit, and a navigation position error $3\sigma = 10\ km$

Small navigation uncertainties ($3\sigma = 10\ km$) lead to the chaser ellipsoid and target tube not intersecting: the probability of collision in this case is infenitesimal if not null. This happens for all chaser orbits within the $4750\ km \leq r_p \leq 5300\ km$ range. For medium navigation errors ($3\sigma = 10\ km$), non-null probabilities start to appear, showcased in the distribution depicted in Figure 6. One must keep in mind that the maximum probability just gives a rough estimate of a maximum threshold for the real probability of collision. The over-estimation of the real probability should be around one or two orders of magnitude, but we can however observe that $P_{c,max}$ dramatically increases when $5050\ km \leq r_p \leq 5125\ km$. In this region, a complementary analysis using continuous probability of collision computations may prove useful to determine wether the risk is viable or not. However, even considering the maximum probability, the value of $P_{c,max} = 6 \cdot 10^{-4}$ is an absolute threshold that seems reasonable, translating into a collisional event happening in average every ~ 450 years (which is far beyond the scope of the 10 revolutions depicted in this study). In order to ensure optimal safety for natural rendezvous operations, the user could also simply choose to pick r_p within the "wells" observed for $P_{c,max}$, namely around $4750\ km \leq r_p \leq 4950\ km$ and $r_p \sim 5000\ km$ for cargo missions, or $r_p \sim 5150\ km$ and $r_p \sim 5250\ km$ for manned missions.

6. CONCLUSION

This work has presented a methodology to fully design natural and safe far-rendezvous transfers between two NRHOs, leading to some conditions on the phasing orbit of the chaser that are dependent on the choice of that target orbit.

It was first established how to generate NRHO-like orbits in the Ephemeris at very little stationkeeping cost, using an innovative long-horizon correction scheme. Then, given a prescribed target orbit, it was established that candidates for a natural far-approach could be exhibited using different methods like local plane search, close-neighbor search or Delauney triangulation. The candidates were consequently classified depending on their location relative to the target orbit, the duration of the approach window and the time interval between two suitable RVD windows. Finally, the last selected candidates were submitted to a safety evaluation check, and some wells for the maximum probability of encounter were exhibited.

These sucessive steps taken alltogether form a robust methodology to construct free natural drift transfers suited to far-rendezvous oeprations. Future work will focus on the transition between close and far rendezvous, at the end of the drift, in order to identify how to initiate most efficiently proximity operations.

7. ACKNOWLEDGMENTS

The authors wish to thank Finn Ankersen and Olivier Mongrard from ESA as well as Francesco Capolupo from Airbus Defence and Space for supporting this work, which was funded under ESA's Network Partnering initiative.

8. REFERENCES

[1] ISECG, "The global exploration roadmap," 2018.

[2] S. Lizy-Destrez, "Rendezvous optimization with an inhabited space station at eml2," in *25th International Symposium on Space Flight Dynamics, ISSFD*, 2015.

[3] D. Guzetti, E.M. Zimovan, K.C. Howell, and D.C. Davis, "Stationkeeping analysis for spacecraft in lunar near rectilinear halo orbits," in *27th AAS/AIAA Space Flight Mechanics Meeting*, 2017.

[4] D.C. Davis, S. Bhatt, K.C. Howell, J.W. Jang, R.J. Whitley, F. Clark, D. Guzetti, E.M. Zimovan, and G. Barton, "Orbit maintenance and navigation of human spacecraft at cislunar near rectilinear halo orbits," in *27th AAS/AIAA Space Flight Mechanics Meeting*, 2017.

[5] J. Williams, D.E. Lee, R.J. Whitley, K.A. Bokelmann, D.C. Davis, and C.F. Berry, "Targeting cislunar near rectilinear halo orbits for human space exploration," in *27th AAS/AIAA Space Flight Mechanics Meeting*, 2017.

[6] S. Manglavitia, A. Campolo, S. Lizy-Destrez, and B. Le Bihan, "Safety analysis for near rectilinear orbit close approach rendezvous in the cislunar realm," in *68th International Astronautical Congress, IAC*, 2017.

[7] W.S. Koon, M.W. Lo, J.E. Marsden, and S.D. Ross, "Dynamical systems, the three-body problem and space mission design," 2017.

[8] W.M. Folkner, J.G. Williams, and D.H. Boggs, "The planetary and lunar ephemeris de 421," Tech. Rep. Vol. 178, Interplanetary Network Progress Report, August 2009.

[9] T.A. Pavlak, "Trajectory design and orbit maintenance strategies in multi-body dynamical regimes," 2013.

[10] J.S. Parker and R.L. Anderson, "Low-energy lunar trajectory design," 2013.

[11] K.C. Howell and J.V. Breakwell, "Almost rectilinear halo orbits," *Celestial Mechanics*, vol. 32, pp. 29–52, January 1984.

[12] D.L. Richardson, "Analytic construction of periodic orbits about the collinear points," *Celestial Mechanics*, vol. 22, pp. 241–253, October 1980.

[13] K.C. Howell, "Three dimensional, periodic, 'halo' orbits," *Celestial Mechanics*, vol. 32, pp. 53–71, January 1984.

[14] G. Wawrzyniak and K. Howell, "An adaptive, receding-horizon guidance strategy for solar sail trajectories," in *AIAA/AAS Astrodynamics Specialist Conference*, 2012.

[15] D.A. Dei Tos, "Automated trajectory refinement of three-body orbits in the real solar system model," 2014.

[16] H. Hinkel, S. P. Cryan, and C. D'Souza, "Rendezvous and docking strategy for crewed segment of the asteroid redirect mission," in *SpaceOps 2014 Conference*, Pasadena, CA, May 2014, American Institute of Aeronautics and Astronautics.

[17] B. Delauney, "Sur la sphère vide," *Bull. Acad. Science USSR VII:Class. Sci. Mat. Nat*, pp. 793–800, 1934.

[18] F.K. Chan, "Spacecraft collision probability," 2008.

[19] S. Alfano, "Determining a probability-based distance threshold for conjunction screening," *Journal of Spacecraft and Rockets*, vol. 50, no. 3, pp. 686–690, May-June 2013.

[20] S. Alfano and D. Oltrogge, "Probability of collision: Valuation, variability, visualization and validity," *Acta Astronautica*, vol. 148, pp. 301–316, 2018.